35. Advances in Planetary Radar Astronomy

Donald B. Campbell[1], R. Scott Hudson[2], and Jean-Luc Margot[3]

[1]National Astronomy and Ionosphere Center/Department of Astronomy, Cornell University
Ithaca, NY 14853-6801 USA
Tel: +1 (607) 255-9580; Fax: +1 (607) 255-8803; E-mail: campbell@astro.cornell.edu

[2]Washington State University, Department of Electrical Engineering
Pullman, WA 99164-2752 USA
Tel: +1 (509) 335-0922; Fax: +1 (509) 335-3818; E-mail: hudson@eecs.wsu.edu

[3]California Institute of Technology
MS 150-21, Pasadena, CA 91125 USA
Tel: +1 (626) 395-6870; Fax: +1 (626) 585-1917; E-mail: margot@gps.caltech.edu

1. INTRODUCTION

During an era when observations from spacecraft have produced the great majority of new information about the solar system, observations of solar-system bodies from the Earth, using high-powered radar systems, have produced some remarkable results. These include the discovery of condensed volatiles, most likely water ice, at the poles of Mercury; the high-resolution imaging of main-belt and near-Earth asteroids, including the discovery of the first near-Earth asteroid binary systems; the discovery of cm-sized grains in the comas of comets; the investigation of the radio-wavelength scattering properties of the surface of Titan; and measurements of the topography of the lunar polar regions at high spatial and altitude resolutions. Multi-wavelength measurements of the scattering properties of the icy Galilean satellites of Jupiter have elucidated some of the properties of their upper surface layers, while measurements of the polarization properties of the echoes from planets, satellites, and small bodies have provided information about their wavelength-scale roughness properties.

It is not possible, in one short review, to discuss both the technical advances in the field of planetary radar astronomy and to describe all the results of their application. Consequently, this paper will concentrate on the technical advances over the past few years, using the results of observations to illustrate their application. Increases in the sensitivity of Earth-based planetary radar systems, especially for the 13-cm wavelength system on the 305-m Arecibo telescope, have been crucial to the recent successes of Earth-based radar astronomy. However, while sensitivity has been very important to the detection and investigation of the bulk-scattering properties of distant bodies such as Titan, to delay-Doppler imaging of the rings of Saturn, and to 15-m resolution delay-Doppler images of near-Earth asteroids, it is a necessary but not sufficient component of efforts to image the surfaces of solar-system bodies. Beginning with the first attempts to image the surface of Venus, radar imaging from the Earth of asteroids, the natural satellites of the planets, and the terrestrial planets (Mercury, Venus, and Mars) has been complicated by "overspread" and range-Doppler ambiguity problems. Both of these problems result in the aliasing of the range-Doppler image for one part of the body onto that from another part, a difficulty not suffered by radar imaging from aircraft or spacecraft, due to the ability of the designers of these systems to tailor the system parameters and antenna beam size to the specific imaging geometry. Much of the technical effort in the field of radar astronomy for the past forty years has been devoted to attempts to overcome these aliasing problems. Over the past few years, these efforts have met with considerable success, and a significant fraction of this paper will be devoted to discussing them.

Much of the current excitement in radar astronomy revolves around observations of asteroids, primarily those near-Earth asteroids (NEAs) that approach within less than 0.1 AU of the Earth. While the technical advances described here have allowed radar astronomers to capitalize on these opportunities, virtually none of it would be possible without the concurrent optical search programs for new NEAs. These programs are crucial to the ability of the radar systems to investigate the diverse properties of these objects.

2. CURRENT EARTH-BASED PLANETARY RADAR SYSTEMS

Figure 1. The 305-m Arecibo telescope.

Four transmitting systems are currently used for radar studies of solar-system bodies. Two of these, a pulsed transmitter at 70 cm wavelength and a continuous-wave (CW) transmitter at

12.6 cm, are on the 305-m Arecibo telescope in Puerto Rico (Figure 1). The Arecibo telescope is operated by Cornell University for the US National Science Foundation. There is a 3.5-cm wavelength CW transmitter on the 70-m NASA Deep Space Network (NASA/DSN) Goldstone antenna in California (Figure 2), and a 6-cm system on the 70-m Evpatoria, Crimea, antenna of the National Space Agency of Ukraine. The two dominant radars in terms of sensitivity are the Arecibo 12.6-cm system and the 3.5-cm Goldstone system, with the Arecibo system being approximately 12 db more sensitive than the Goldstone system for a single observation. However, the Arecibo antenna's maximum zenith angle of 20° limits its declination coverage to roughly 1° S to 39° N. The greater declination coverage and longer tracking time of the Goldstone 70-m antenna makes its radar system very competitive with Arecibo's in such areas as the imaging of near-Earth asteroids. Table 1 gives the specifications of the monostatic radar systems on the three antennas, and also gives the locations and specifications of the main antennas that are used in conjunction with these radars to form bistatic or radar-interferometric systems.

Figure 2. The 70-m Goldstone telescope.

During the mid-1990s, the 305-m Arecibo telescope and its 2380 MHz CW radar system underwent a major upgrading. The optics of the telescope were modified to use a pair of shaped reflectors, instead of line feeds, to correct for the telescope's spherical aberration [*Kildal et al., 1994*]. This resulted in more-efficient illumination of the primary reflector and, hence, greater gain at 13 cm and other wavelengths. The reflectors also provide an offset illumination of the primary

Table 1a. Current planetary radar systems associated with radio-astronomy installations.

Location	Lat. (° ′)	E. Long. (° ′)	Frequency (GHz)	Transmitter Type & Power (kWatts)	Antenna Gain (dB)	System Temp. (K)
Arecibo[1] Puerto Rico	18 21	-66 45	0.430	Pulse 150 avg 2,500 peak	61	55
Arecibo[1] Puerto Rico	18 21	-66 45	2.380	CW 1,000	73.4	26
Goldstone California	35 23	-116 51	8.560	CW 470	73	14
Evpatoria Crimea	33 11	45 11	5.01	CW 150	69	45

Table 1b. Main auxiliary receiving antennas for the CW radar systems shown in Table 1a.

Location	Receiving Locations	Antenna Type
Arecibo[1] Puerto Rico	Green Bank, W. Virginia[2], USA Goldstone, California, USA St. Croix to Hawaii, USA	100 m Dish 70 m and 34 m Dishes VLBA (10 × 25 m Dishes)
Goldstone California	Socorro, New Mexico, USA Green Bank, W. Virginia[2], USA	VLA (27 × 25 m Dishes) 100 m Dish
Evpatoria Crimea	Effelsberg, Germany Medicina, Italy	100 m Dish 32 m Dish

Notes: [1]The Arecibo telescope can point up to 20° from the vertical. The parameters are for zenith pointing. [2]Considerable use is anticipated.

reflector, delaying until 15° the zenith angle at which the 215 m × 235 m illuminated area spills over the edge of the fixed primary reflector. For zenith angles greater than 15°, there is a gradual reduction in gain, amounting to -1 db at the maximum tracking zenith angle of 20°. A 15-m high "ground screen" (see Figure 1) around the perimeter of the primary reflector further delays to 18.5° the zenith angle at which the illuminated area spills onto the surrounding (300 K) terrain. This results in an almost constant system temperature with zenith angle, a considerable improvement compared with the almost tripling of the system temperature between 11° and 20° when a line feed was used. At zenith, the system temperature at 13 cm, when viewing the cold sky, declined from 34 K to 26 K, due to the elimination of ohmic losses in the line feed. Finally, the power of the 13-cm wavelength transmitter was increased from 420 kW to 1,000 kW by utilizing two Varian (now CPI) VKS 8270A amplifying klystrons. All of these improvements resulted in an increase in the system's sensitivity for most planetary radar observations of a factor of eight when the telescope is looking at the zenith, and a factor of over 30 when looking at the telescope's maximum zenith angle of 20°. Further improvements, primarily in the system temperature and the telescope's focus adjustment, are expected to increase the sensitivity by an additional factor of 1.2 (1 db) by the end of 2002.

Over the past few years, only relatively minor improvements have been made to the sensitivity of the Goldstone 3.5 cm radar system. New CPI klystrons have provided slightly increased transmitter power. Goldstone's 3.5 cm maser amplifiers provide an impressive 14 K system temperature at zenith and cannot be significantly improved upon. There were also no significant changes in the Evpatoria 6 cm system. There are plans to change the frequency of this system to 8.5 GHz and to increase the power to 500 kW, but these plans are waiting on funding.

For a given radar system, the achievable spatial resolution on a target is determined primarily by the inverse fourth power of its distance, with lesser dependencies on its rotation period and reflection properties. For asteroids or comets approaching within 0.05 AU of the Earth, the upgraded Arecibo system can obtain delay-Doppler images with approximately 15 m resolution in delay (0.1 μsec time resolution) and, depending on the rotation period, equivalent or better resolution in the Doppler dimension. The Goldstone system can achieve similar resolutions out to approximately 0.03 AU. Arecibo is limited by the 25 MHz bandwidth of the transmitter's klystrons to time resolutions ≥ 0.05 μsec or 7 m delay resolution. Time resolutions of 0.05 μsec imply (complex) sampling rates of 20 MHz per received polarization. Direct-sampling systems, operating at these rates, have recently been installed at both Arecibo and Goldstone, providing an output stream of 20 MB/sec. The recent increases in disk storage capacity, I/O rates, and computing power are making direct-sampling systems, storage, and subsequent analysis more attractive than constructing special-purpose processors. While the cross-correlation and transform operations on the data cannot yet be performed in real time at the maximum data rates using relatively cheap workstations, projected improvements in computing speed may make this a real possibility in the near future.

Over the past five years, there has been a significant increase in the use of multiple-antenna systems, primarily, as will be discussed in the next section, to resolve the various aliasing problems associated with the standard delay-Doppler mapping technique used to image planets and asteroids, or for altimetry measurements using radar interferometric techniques. *Margot et al.* [*1999a*, *b*; *2000a*] used the Goldstone radar and several 34 m receiving antennas at the Goldstone site as a radar interferometer to measure the topography of Tycho crater, and the polar regions of the Moon, with 150 m spatial and 50 m height resolutions. *Margot and Nolan* [*1999*] used Arecibo in conjunction with the NASA/DSN 70 m Madrid antenna in an attempt to use interferometry to unambiguously image the near-Earth asteroid (NEA) 6489 Golevka. In May, 2001, they carried out a similar experiment, using the Goldstone 70 m antenna as an interferometric receiving antenna in an attempt to image the 1.2 km diameter NEA 2000 KW4. *Black et al.* [*1999*] have carried out initial test observations of two NEAs using Goldstone or Arecibo to transmit and the Very Long Baseline Array – ten 25 m antennas, located between Hawaii and St Croix – as a radar-synthesis imaging system with, potentially, resolutions of less than 100 m for NEAs approaching within 0.03 AU of the Earth. *Harcke et al.* [*2001*] are using the Very Large Array (VLA) in New Mexico to synthesize images of the icy Galilean satellites, illuminated by the Goldstone transmitter. *Slade et al.* [*2001*] used Arecibo to transmit at 2.38 GHz, and several antennas at the Goldstone site in California as a radar interferometer, to measure altitudes near the sub-Earth point on Venus. Absorption in the Venus atmosphere precludes using the Goldstone 8.5 GHz transmitter for this purpose. However, *Jurgens et al.* [*2001*] are using the Goldstone radar and the 34 m antennas at the Goldstone site to image the sub-Earth region on Mars as the planet rotates. In the first scheduled use of the new 100 m Green Bank Telescope (GBT), in West Virginia, USA, *Campbell et al.* [*private communication*] used Arecibo to transmit to Venus and Arecibo, and the GBT as a receiving radar interferometer, with the aim of measuring altitudes over Maxwell Montes, an elevated region with a very high Fresnel reflectivity and very low emissivity. The GBT will be an important ancillary antenna for both the Arecibo and Goldstone radars for observations of slowly rotating NEAs and comets. For such targets, the round-trip-light time is so small – typically, less than 20 sec – that the resolution in the Doppler-broadened spectrum achievable with the short burst of data is comparable to or smaller than the total Doppler broadening, preventing resolution in this dimension in any delay-Doppler image. A bistatic observation provides long data streams. *Zaitsev et al.* [*private communication*] made bistatic observations of the NEA 1998 WT24, which approached to within 0.012 AU of the Earth in December, 2001, with Evpatoria transmitting, and the 32 m Medicina, Italy, antenna receiving the echo.

3. IMAGING IN RADAR ASTRONOMY

Most imaging of planetary and smaller bodies in the solar system with Earth-based radars has relied on the delay-Doppler technique, the discrimination of echo power in intervals of time delay and Doppler shift. However, delay-Doppler imaging with Earth-based radars is plagued by two problems that are relatively easily dealt with for aircraft and spacecraft-borne imaging radars: overspread, and delay-Doppler ambiguities. Overspread is a sampling-rate aliasing problem. For imaging a target body, which, on reflection, time-disperses an incident short pulse over $\delta\tau$ s, the time between transmitted pulses – if a pulsed transmitter is used (or the repetition period of a binary PN phase code, for a phase-coded CW transmission) – must be at least $\delta\tau$ s if range aliasing is to be avoided. However, a (complex) sampling rate of $\delta\tau$ can only fully represent a signal with a bandwidth of less than $1/\delta\tau$ Hz. If the Doppler broadening induced by the target's rotation is larger than $1/\delta\tau$, then aliasing will occur in the frequency domain. The Doppler broadening of the received echo from a rotating target is given by

$$\delta B = 8\pi r \nu \cos i / Pc \ \text{Hz}, \tag{1}$$

where *r* is the radius, ν is the transmitter frequency, *P* is the apparent rotation period looking from the Earth, *c* is the velocity of light, and *i* is the angle between the rotation axis and the normal to the line of sight from the Earth. The requirement for the echo from a target to not be overspread is $\delta\tau\, \delta B \le 1.0$.

At the wavelengths of the Arecibo and Goldstone radar systems, 12.6 cm and 3.5 cm, respectively, the terrestrial planets, the Galilean satellites of Jupiter, Titan, and the large main-belt asteroids, Ceres and Pallas, are all overspread. Venus, at 12.6 cm, is only just overspread at inferior conjunction, with $\delta\tau\, \delta B \cong 1.3$, allowing delay-Doppler mapping for most of the surface visible at inferior conjunction. At this wavelength, Mercury is overspread by a factor of 1.6 at inferior conjunction, allowing for some delay-Doppler mapping, while Mars is overspread by a factor of 170. The rings of Saturn are so overspread – by a factor of about 10^6 – that a delay-Doppler image with adequate resolution in both dimensions can only be obtained from a single transmitted pulse, in a technique called intrapulse mapping. This will be discussed in more detail below.

The delay-Doppler ambiguity problem arises from there being two or more points on the target's surface that are at the same distance from, and have the same relative velocity with respect to, the radar. Consequently, it is impossible, with a simple radar system using an antenna with a beamwidth larger than the target (the case for all solar-system objects, except the Moon), to discriminate between the echo power from these "ambiguity" points. Large solar-system bodies, such as the terrestrial planets, Galilean satellites of Jupiter, Titan, etc., are very close to spherical. They have a twofold ambiguity, with the ambiguity points located symmetrically north and south of the apparent Doppler equator (the equator defined by the projected apparent rotation axis, looking from the radar), and equidistant on the plane of the sky from the apparent rotation axis. Hence, the term N(orth)-S(outh) ambiguity. For irregular, solid objects, such as small main-belt or near-Earth asteroids, a given location may have the same distance and velocity as none, one, or more other locations. The requirement for the same velocity dictates that all points that are ambiguous with each other are equidistant on the plane of the sky from the projected apparent rotation axis.

3.1 DELAY-DOPPLER MAPPING AND THE CODED LONG PULSE TECHNIQUE

Traditional delay-Doppler mapping, for studies of solar system bodies, has utilized either a train of coherent pulses, separated by $\delta\tau'$ s (a pulsed transmitter) or, more commonly, the phase modulation of a CW-transmitted waveform, using a cyclic PN binary shift register code with a repetition time for the code of $\delta\tau'$ s. Both the Arecibo and Goldstone systems use a phase-coded transmission, in order to maximize average transmitted power. For coded transmissions at each basic time interval, the baud interval, the phase of the transmitted signal is reversed or not, depending on the code. The baud interval is the basic time resolution of the system, and is typically between 0.1 μsec and 10 μsec, depending on the application. The cross correlation of the cyclic code with one code cycle is strongly peaked at zero lag and at lags corresponding to multiples of the code length, and has extremely low values at other lags. Cross-correlating the received echo with a replica of the transmitted code discriminates echo power as a function of time delay within each code cycle. Fourier-transforming the lag products corresponding to a specific time delay – relative to, say, the leading edge of the target – for a sequence of *n* code cycles, provides echo power as a function of Doppler frequency and time delay. The resolution in the Doppler dimension is given by $\Delta\nu = \left(n\,\delta\tau'\right)^{-1}$ Hz, where $\delta\tau' = l\Delta t$ s, with l being the code length, and Δt being the baud interval. The ambiguity function – basically, the echo power as a function of time and frequency, after reflection from a point target – is repetitive in time every $\delta\tau'$ s, and in frequency, every $1/\delta\tau'$ Hz. Since the ambiguity function convolves the target-scattering function, $\sigma\left(\tau,\nu\right)$, it is clear that $\delta\tau\;\delta B \le 1.0$ is required to avoid overspread, aliasing in time or frequency.

For those solar-system objects that are not overspread, delay-Doppler imaging is a very powerful technique for imaging their surfaces. Recent notable examples are the Arecibo imaging of the polar caps of the Moon [*Stacy et al.*, *1997*], and the imaging by both Arecibo and Goldstone of numerous NEAs. These include 1999 JM8 (Figure 3), and four that were discovered from the delay-Doppler images to be binary systems (Figure 4), the first confirmed NEA binaries [*Ostro et al.*, *2000a*; *Margot et al.*, *2000b*; *Nolan et al.*, *2000*; *Benner et al.*, *2001a*; *Benner et al.*, *2001b*; *Margot et al.*, *2002*]. While, as discussed below, full-disk imaging of Mercury, using radar aperture synthesis or the coded long pulse technique, were instrumental in the discovery and initial mapping of the ice deposits at the poles of Mercury, they can also be studied using simple delay-Doppler mapping. Figure 5 shows an Arecibo delay-Doppler image of Mercury's northern polar region, made at a resolution of 1.5 km. Because of their very high backscatter cross sections, even at 80° incidence angle, the ice deposits are clearly visible, while virtually no signal is detectable from the surrounding terrain.

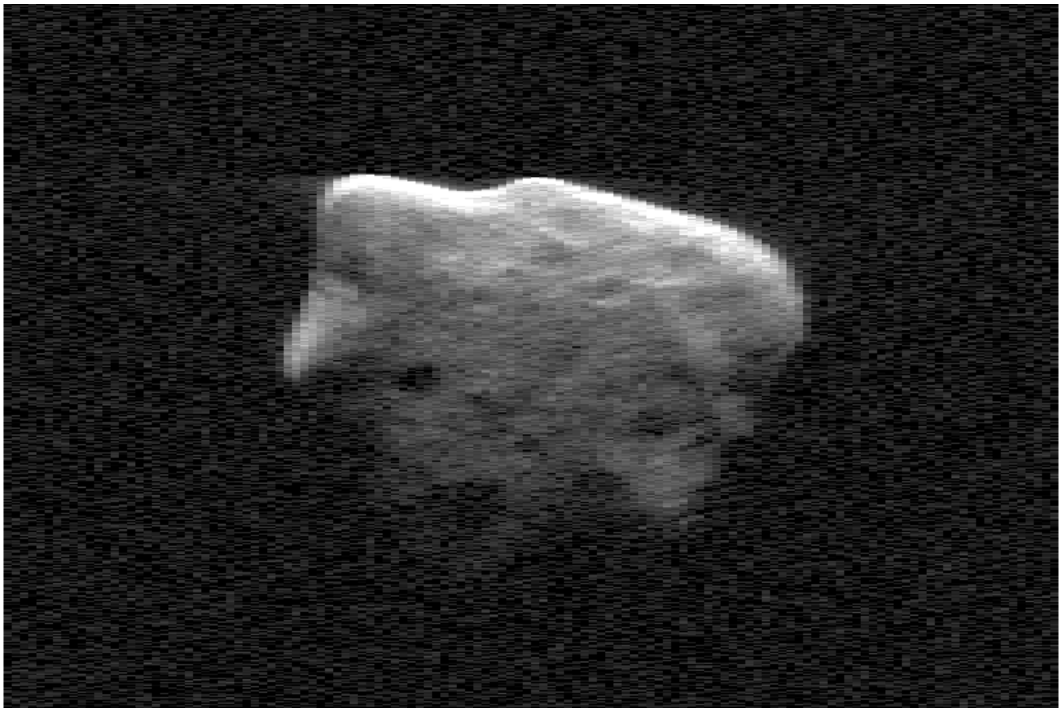

Figure 3. An Arecibo delay-Doppler radar image of the NEA 1999 JM8, made on August 5, 1999, when it was at a distance of 9×10^6 km from the Earth. JM8 has a size of approximately 3 km, and the resolution of the image in both delay and Doppler is about 15 m [*Benner et al.*, *2001c*].

Planetary radar observations are not the only ones to suffer from overspread problems. Incoherent-scatter radar observations of intermediate levels in the Earth's ionosphere are also overspread by a small factor, which prevents adequate time and frequency resolution using the intrapulse technique, but is sufficiently aliased that useful results cannot be obtained by simple delay-Doppler pulse-to-pulse coherent processing. *Sulzer* [*1986*] suggested and implemented what is called the coded long pulse (CLP) technique, in which a long, non-repeating, binary phase code is used. As discussed above, normal delay-Doppler processing involves cross correlation of the received echo with a replica of the transmitted cyclic code and Fourier transformation using the appropriate lags for each code cycle. In the CLP technique, the incoming echo is multiplied by a replica of the long transmitted code, with a lag corresponding to the desired delay, and a transform performed on the resultant lag products. These are spaced at the baud interval, Δt, giving an unaliased bandwidth of $1/\Delta t$ Hz, as opposed to the unaliased bandwidth of $1/l\Delta t$ Hz for normal delay-Doppler mapping. The disadvantage of this technique is that for each delay echo, power

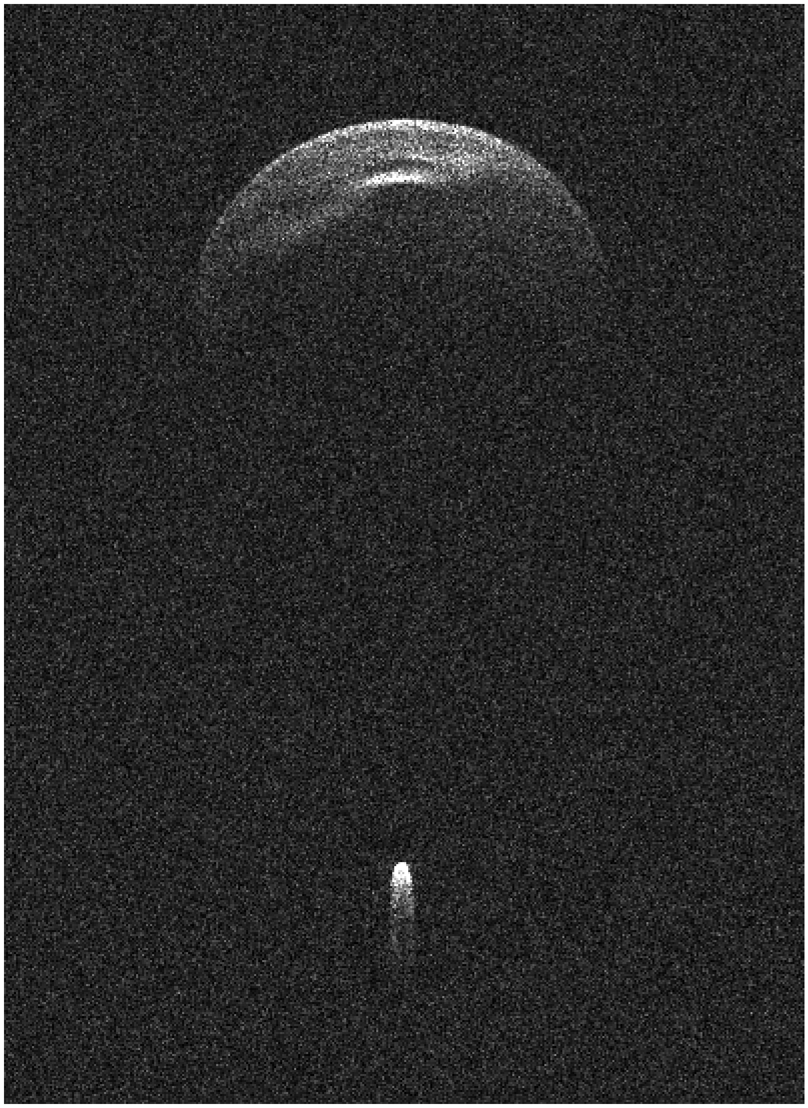

Figure 4. An Arecibo delay-Doppler image of the binary NEA 1999 KW4, made on May 26, 2001, at a resolution of 8 m. The diameter of the primary body is about 1.2 km, while the size of the secondary is approximately 400 m. KW4 was at a distance of 3×10^6 km when this image was made [image courtesy of S. J. Ostro, J. L. Margot, and collaborators].

from all the other unwanted delays is included as a randomized noise clutter signal. This arises because for each of the other delays, the reflected signal is multiplied by the code at a lag determined by the number of baud intervals to the wanted delay. This randomizes the phase from this delay for each baud interval, so that the output from the Fourier transform is noise-like. The contribution of the sum of these noise-like contributions from all the other delays adds to the noise contribution from the receiving-antenna's system temperature, and clearly puts an upper limit on achievable signal-to-noise, no matter how sensitive the radar system. A detailed description of the coded long pulse technique, and its application to radar observations of solar-system objects, can be found in *Harmon* [*2001*]. A slightly different approach was suggested by *Hagfors and Kofman* [*1991*], using a Gaussian-noise modulation, instead of a long binary PN shift-register code. This technique has not yet been applied to planetary studies.

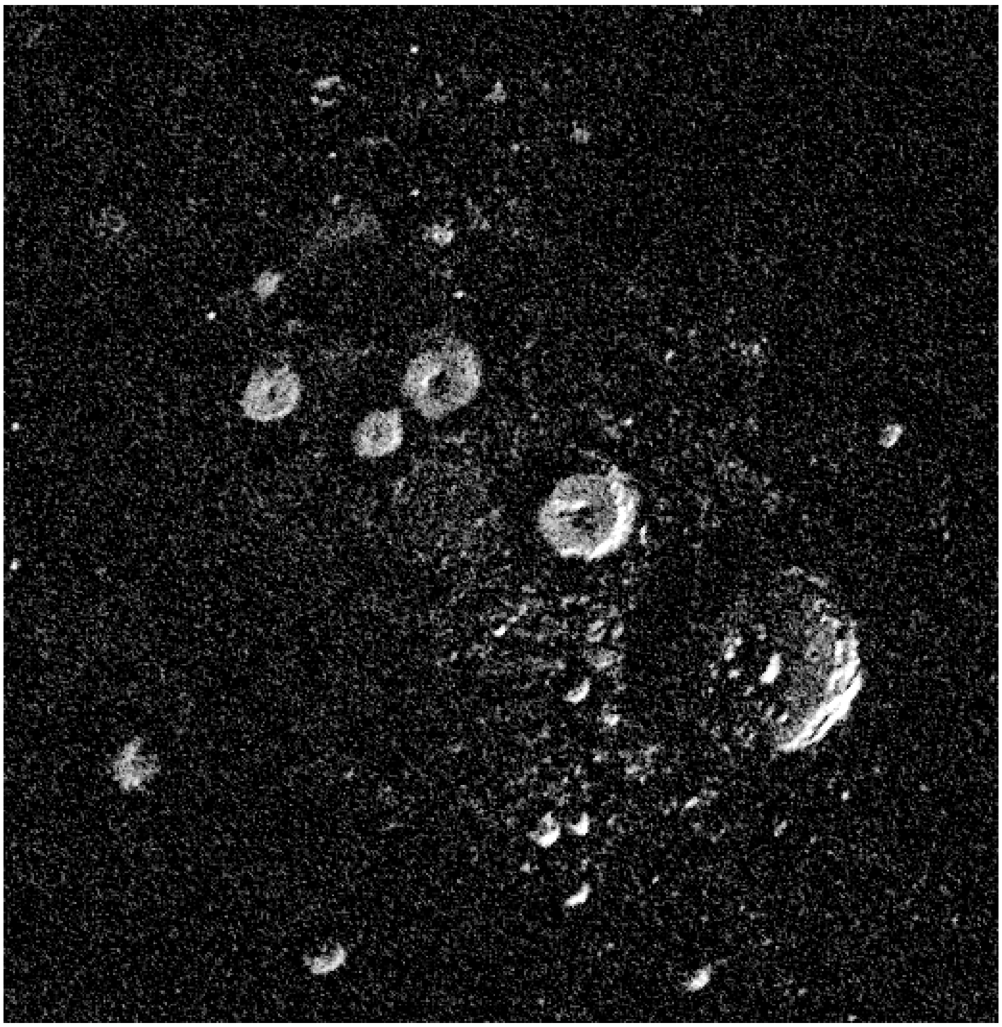

Figure 5. An Arecibo delay-Doppler image, from *Harmon et al.* [*2001*], of the north pole of Mercury, showing the probable ice deposits. A 10 µsec baud length was used, giving a resolution of 1.5 km. The image, which was made on July 25/26, 1999, covers an area of approximately 300 km × 300 km. The pole is located just below the small of the three craters slightly above and left of the center of the image.

In 1990, *Harmon et al.* [*1992*] first applied the CLP technique to Mars, using the Arecibo 2.38 GHz radar system. At this frequency, Mars has an overspread factor of 170, making normal delay-Doppler mapping impossible, except for a very small area around the sub-radar point at the center of the visible disk. Since that time, it has been applied to additional imaging of Mars during the opposition of 1992/1993 [*Harmon et al.*, *1999*], to full-disk imaging of Mercury [*Harmon and*

Slade, *1992*; *Harmon*, *1997*], to ranging and imaging of the icy Galilean satellites of Jupiter [*Harmon et al.*, *1994*; *Harcke et al.*, *2001*], and to the imaging of the main-belt asteroid 216 Kleopatra [*Ostro et al.*, *2000b*].

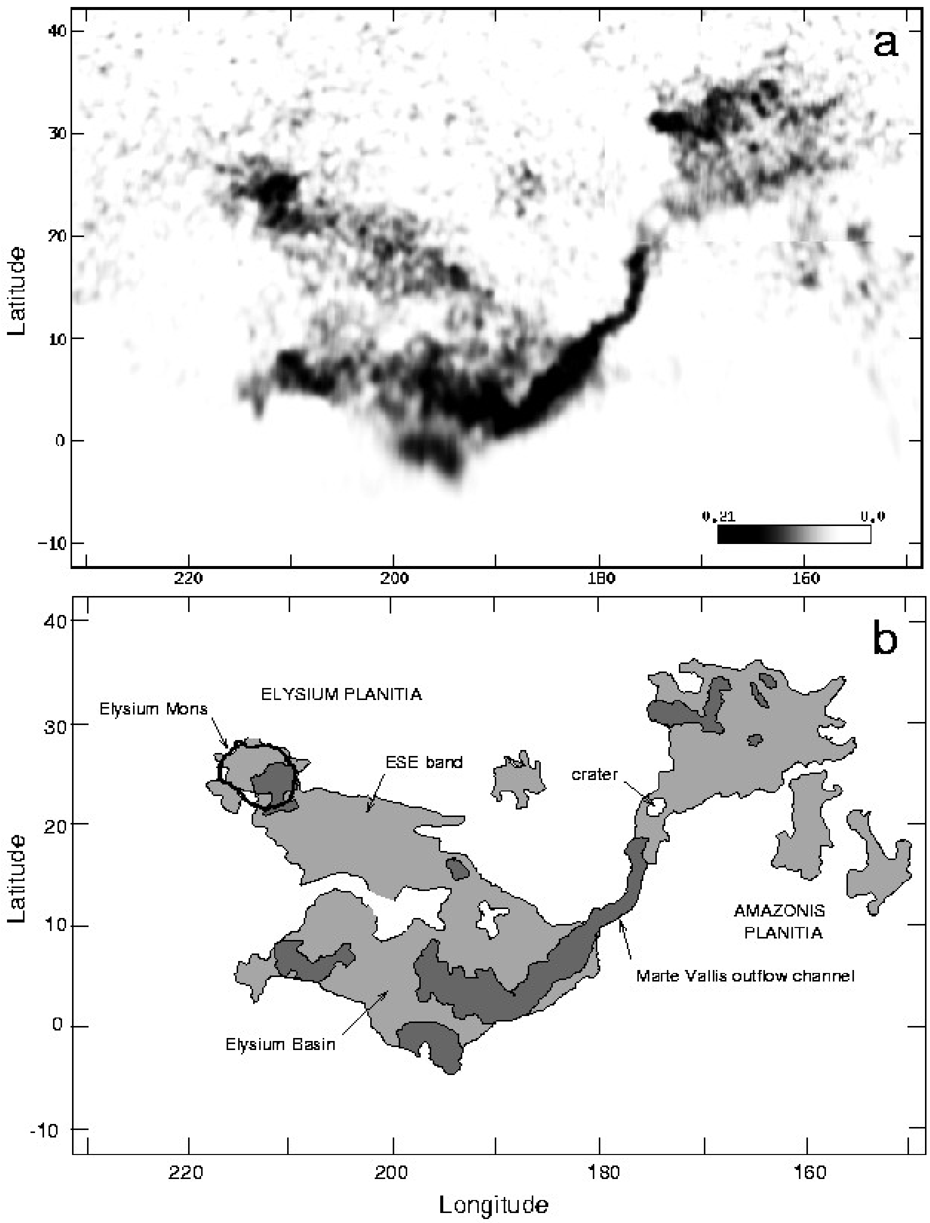

Figure 6. An Arecibo radar image of the Elysium region on Mars, made using the CLP technique, and an accompanying sketch map based on the image. Darker shades indicate areas of higher backscatter cross section. The high backscatter return from the Marte Vallis outflow channel suggests that the channel may be surfaced with rough lava flows [*Harmon et al.*, *1999*].

To date, the two great successes of the CLP technique have been the imaging of Mercury and Mars. It was the full-disk CLP imaging of Mercury with Arecibo [*Harmon and Slade*, *1992*] that provided the confirming observations at significantly higher resolution of the putative ice deposits at the north pole of Mercury, discovered with the Goldstone/VLA synthesis imaging system (see below). Since radar is sensitive to wavelength-scale structure, the CLP delay-Doppler images of Mars have played an important role in delineating the locations of rough lava flows, including flows in the Elysium basin and outflow channel [*Harmon et al.*, *1999* and Figure 6].

3.2 INTRAPULSE MAPPING OF SATURN'S RINGS

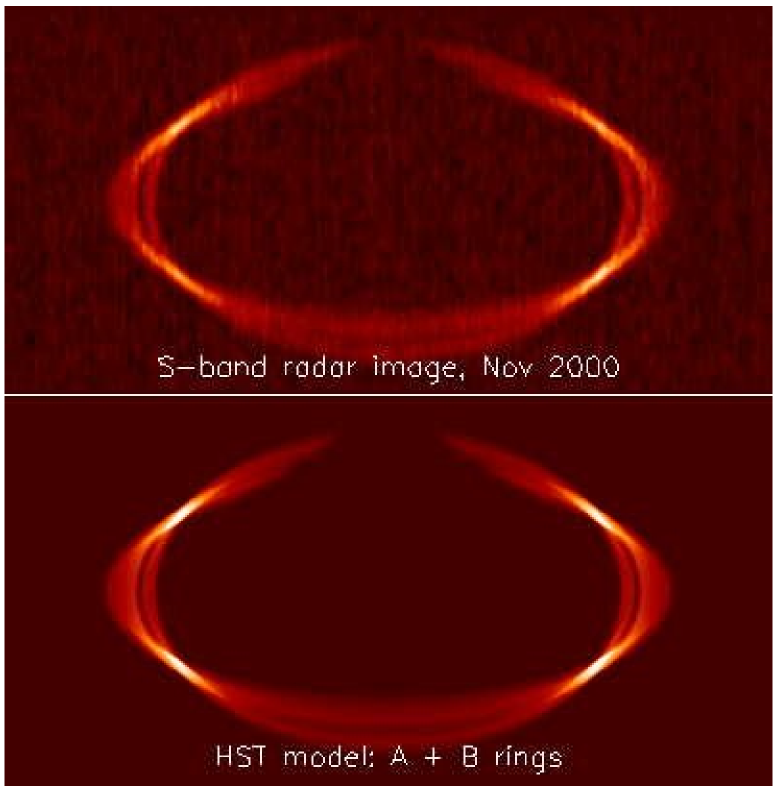

Figure 7. An Arecibo delay-Doppler radar image of Saturn's rings, from intrapulse observations made in November, 2000. Twenty-four frequency hops were used. The pulse length was 75 ms (11,000 km range resolution), and the processing Doppler-frequency resolution was 2 kHz, corresponding to a spatial resolution of about 2,000 km near the ansae. Also shown is a model delay-Doppler image based on a Hubble Space telescope image made at the same time. Only the optical image of the A and B rings was used, and it was assumed that the radar backscatter cross section mimics the visible-wavelength optical depth [image courtesy of P. D. Nicholson] (also see Plate 15).

The ambiguity function of a single transmitted RF pulse has a width of $\sim \Delta t$ s in the time dimension, where Δt is the pulse length, and $1/\Delta t$ Hz in the frequency dimension. Consequently, for a greatly overspread target – such as Saturn's rings, where the inverse of the desired (or achievable from a signal-to-noise consideration) time resolution is small compared with the

Doppler broadening – then a delay-Doppler image can be obtained from a single pulse. Signal-to-noise is enhanced by an incoherent summation of images from a sequence of transmitted pulses, separated by at least the delay depth of the rings. For a CW transmitter, it can be further enhanced by stepping the transmitter frequency after each pulse by an amount larger than the Doppler broadening, and transmitting another pulse. A total of $\delta\tau/\Delta t$ steps can be made, where $\delta\tau$ is the delay depth of the target, provided the allowable bandwidth of the transmitter is greater than the number of steps times δB, the Doppler bandwidth of the target. For an optimized system, the number of pulses, *N*, that can be transmitted is the observing time divided by Δt, and the signal-to-noise enhancement is $N^{1/2}$.

Intrapulse imaging can be used effectively on only two solar-system objects, Saturn's rings and the Sun. With a diameter between the outer edges of the A ring of 274,000 km, giving a delay depth of between 1.6 s and 1.8 s (depending on their inclination) and a Doppler broadening at 2.38 GHz of ~ 700 kHz, the rings are overspread by a factor of $\sim 10^6$. Low signal-to-noise intrapulse imaging observations of the rings were made by *Ostro et al.* [*1982*] in 1980, transmitting a 400 ms long pulse at a repetition period of 3.2 sec with the Arecibo 2.38 GHz radar, and receiving with both the Arecibo and Goldstone antennas. Eight frequency steps were used. In 1999, *Nicholson et al.* [*2000*] used the upgraded Arecibo radar to transmit 100 ms long pulses every 2.2 sec at each of 12 frequencies. This pulse length gave a delay resolution of 15,000 km, and the data were processed in frequency to give a resolution in the Doppler dimension of 2,000 km. Nicholson et al. repeated these observations in 2000 at a different ring-inclination angle, using a pulse length of 70 ms and 24 frequencies. Figure 7 shows the delay-Doppler image, compared with an equivalent image synthesized from almost simultaneous Hubble Space Telescope observations. The image shows a clear azimuthal asymmetry in the ring-particle cross section, which is thought to be related to wakes resulting from gravitational clumping of particles, and subsequent shearing due to the gradient in the Keplerian velocity with distance from Saturn.

3.3 Physical Modeling of Asteroids from Delay-Doppler Data

One of the major advances in planetary radar astronomy over the past few years has been the development of inversion techniques, which allows a three-dimensional representation of a body to be obtained from a set of (aliased) delay-Doppler images. The somewhat non-intuitive geometry of delay-Doppler images, compounded by aliasing problems, limits our ability to make direct physical inferences from such images. In fact, interpreting them with a "visual-image mind set," can lead to very erroneous conclusions. Even in the case of optical images, it is desirable to "invert" one or more two-dimensional images to arrive at a three-dimensional model of the object, since many scientific investigations, such as the study of gravitational properties and impact dynamics, are facilitated by a three-dimensional model. Therefore, effective techniques for delay-Doppler image inversion are necessary to realize the full scientific potential of radar-image technology.

The goal is to invert a sequence of delay-Doppler images to arrive at a physical model of the object under study. Toward this end, a suitable mathematical model is adopted of the shape, photometric properties, spin, and orbital dynamics of the object, in terms of a set of discrete parameters, $\vec{p}$. The observed data are then used, via a weighted-least-squares fit, to determine that

$\vec{p}$ which best represents the real object. A detailed description of the inversion technique can be found in *Hudson* [*1993*]. The following is a schematic outline.

Given a physical model, described by shape, photometric, spin, and orbital parameters, $\vec{p}$, modeled delay-Doppler images are computed from

$$I_{ijk}^{\text{mod}}(\vec{p}) = \iint_s V(u,v;k)\, h_\tau\left[\tau_i - \tau(u,v;k)\right] h_f\left[f_j - f(u,v;k)\right] \sigma_0(u,v;k)\, du\, dv\,. \qquad (2)$$

Here, coordinates u and v denote position on the surface, while i and j index delay and Doppler pixels, respectively, and k indexes different images. V is the visibility function, which is unity if the point at u,v is visible to the radar, and zero otherwise. h_τ, h_f are the radar impulse responses in delay and Doppler, while $\tau(u,v;k)$, $f(u,v;k)$ are the delay and Doppler coordinates of the surface point u,v for each k. Finally, $\sigma_0(u,v;k)$ is the differential cross section, which gives the amount of power backscattered per unit surface area. $V(\ ), \tau(\ ), f(\ ), \sigma_0(\ )$ are all implicit functions of $\vec{p}$.

The χ^2 goodness-of-fit measure for a particular model is

$$\chi^2(\vec{p}) = \sum_k \sum_{ij} \left(\frac{I_{ijk} - I_{ijk}^{\text{mod}}(\vec{p})}{\sigma_{ijk}} \right)^2, \qquad (3)$$

with σ_{ijk} being the standard deviation of noise in the *ij* pixel of image k, and I_{ijk} being the observed data. That $\vec{p}$ which gives the smallest χ^2 therefore represents the "most-likely" model. However, there are usually problems with simply minimizing χ^2 with respect to $\vec{p}$ to arrive at a model. First of all, the solution may not be unique. An obvious case is where some fraction of the body's surface was never visible to the radar. Alternately, there could be some geometric weakness in the data set with respect to resolving the N-S ambiguity. Therefore, it is a better idea to form and minimize an "objective function" by adding "penalty" terms, as in

$$O(\vec{p}) = \chi^2(\vec{p}) + \sum_{m=1}^{M} w_m R_m(\vec{p})\,. \qquad (4)$$

Here, $R_m(\vec{p})$ is a function that "penalizes" some attribute of the model, and w_m is a factor that weights how strongly this penalty is taken into account. For example, $R_m(\vec{p})$ can measure the "non-smoothness" of the surface, and increasing w_m will force the model to become smoother, typically at the expense of an increase in χ^2. Minimizing $O(\vec{p})$ for different values of w_m allows us to see how χ^2 varies with w_m, that is, how strongly the modeled data depend on the particular physical property being penalized. Clearly, if some feature of a model can be suppressed in this manner without causing a statistically significant increase in χ^2, the presence of the feature on the actual body is very doubtful. By using penalty terms in this way, we can "push" the model around, and arrive at an understanding of how well it is constrained by the observed data, and gain confidence in those aspects of the model that cannot be suppressed without a statistically significant increase in χ^2.

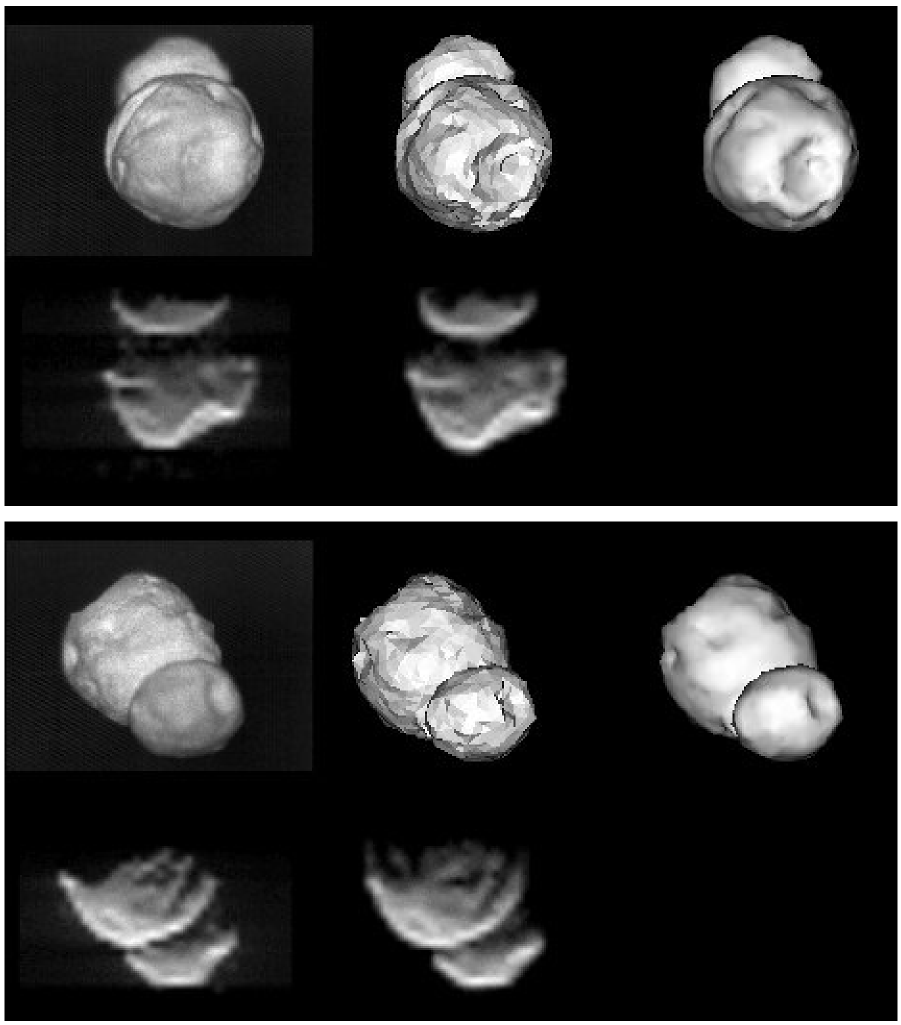

Figure 8. A laboratory shape-reconstruction experiment for a clay model. The model accurately represents the body to the limits of the delay-Doppler image resolution. The two frames represent two views of the object, model, and delay-Doppler images. In each frame, the three images in the top row show, respectively, the object, the surface-facet reconstruction, and a smoothed version of the reconstruction. The bottom two images show the observed and modeled delay-Doppler images [*Andrews et al.*, *1995*].

Because the delay-Doppler inversion problem can be ill-posed, and because it is based on a necessarily simplified mathematical model of radar scattering, it is important to study any inversion technique with test cases, where the true solution is known in advance. Ideally, we would be able to do this with real asteroids for which both radar and spacecraft flyby or rendezvous data sets are available, but such test cases are not currently available. Instead, *Andrews et al.* [*1995*] have described a laboratory laser-radar system that serves as a scale model of a planetary radar. Using this system, optical "delay-Doppler" data sets have been obtained for clay-model "asteroids," and inversion techniques have been tested. In general, it has been found that computed models are accurate over the imaged regions of an asteroid, provided a sequence of delay-Doppler images is available that has good rotational-phase coverage, and is not limited to the equatorial plane of the body. An example is shown in Figure 8.

The effectiveness of the inversion technique and the number of bodies, primarily NEAs, to which it has been applied over the past few years have paralleled the increasing rate of NEA discoveries – especially, NEAs that approach within 0.05 AU of the Earth – and the increasing spatial resolution of the delay-Doppler imagery. The first application of the technique was to Arecibo delay-Doppler images of the approximately 1-km-sized bifurcated NEA 4679 Castalia [*Hudson and Ostro*, *1994*]. Since then, three-dimensional reconstructions have been obtained for, among others, the NEAs 4179 Toutatis [*Hudson and Ostro*, *1995*], 6489 Golevka [*Hudson et al.*, *2000a*], and 1999 RQ 36 [*Hudson et al.*, *2000b*], and the main-belt object 216 Kleopatra [*Ostro et al.*, *2000b*]. Figure 9 gives the results of the inversion of the radar-image data for five NEAs and Kleopatra.

Various problems can complicate the inversion process, including non-principal-axis rotation and poor signal-to-noise ratios. Included in the parameters to be fit is the spin vector, since it is normally either unknown or poorly known. While most asteroids are rotating about their principal axes, this is not always the case. Toutatis was the first example of an NEA where the inversion was complicated by non-principal-axis rotation [*Hudson and Ostro*, *1995*]. From the fit, it was determined to have a rotation period of 5.41 days, and a precession period of 7.35 days. Delay-Doppler images with relatively low signal-to-noise ratios – as was the case for Kleopatra, at a distance of 1.1 AU from the Earth – are amenable to inversion provided that adequate aspect-angle coverage is obtained. Figure 10 shows a series of delay-Doppler images for Kleopatra, the resultant projected-shape model for the aspect angle corresponding to each delay-Doppler image, and the reconstructed delay-Doppler images based on the shape model. While there are still significant uncertainties in both the exact shape and size of Kleopatra [*Ostro et al.*, *2000b*], the overall shape of Kleopatra is correct, and this is an impressive example of the power of radar imaging combined with the inversion technique.

3.4 Synthesis Imaging

Direct synthesis imaging of a radar-illuminated solar-system body provides plane-of-sky images without any of the problems – overspread and range-Doppler ambiguities – that plague delay-Doppler imaging. In its simplest application, this technique uses the radar signal to raise the effective brightness temperature of the body, and a synthesis interferometer to image the "source." In 1988, *Muhleman et al.* [*1991*] imaged Mars by transmitting a CW signal with the 3.5 cm Goldstone radar, and using the 27 antennae of the Very Large Array (VLA) to synthesize an image of the planet. The VLA was configured to have its maximum extent, the A array, giving a width for the synthesized beam of 0.24", corresponding to ~ 90 km at the distance of Mars at opposition. This highlights the disadvantages of radar-synthesis imaging. While the images do not suffer from

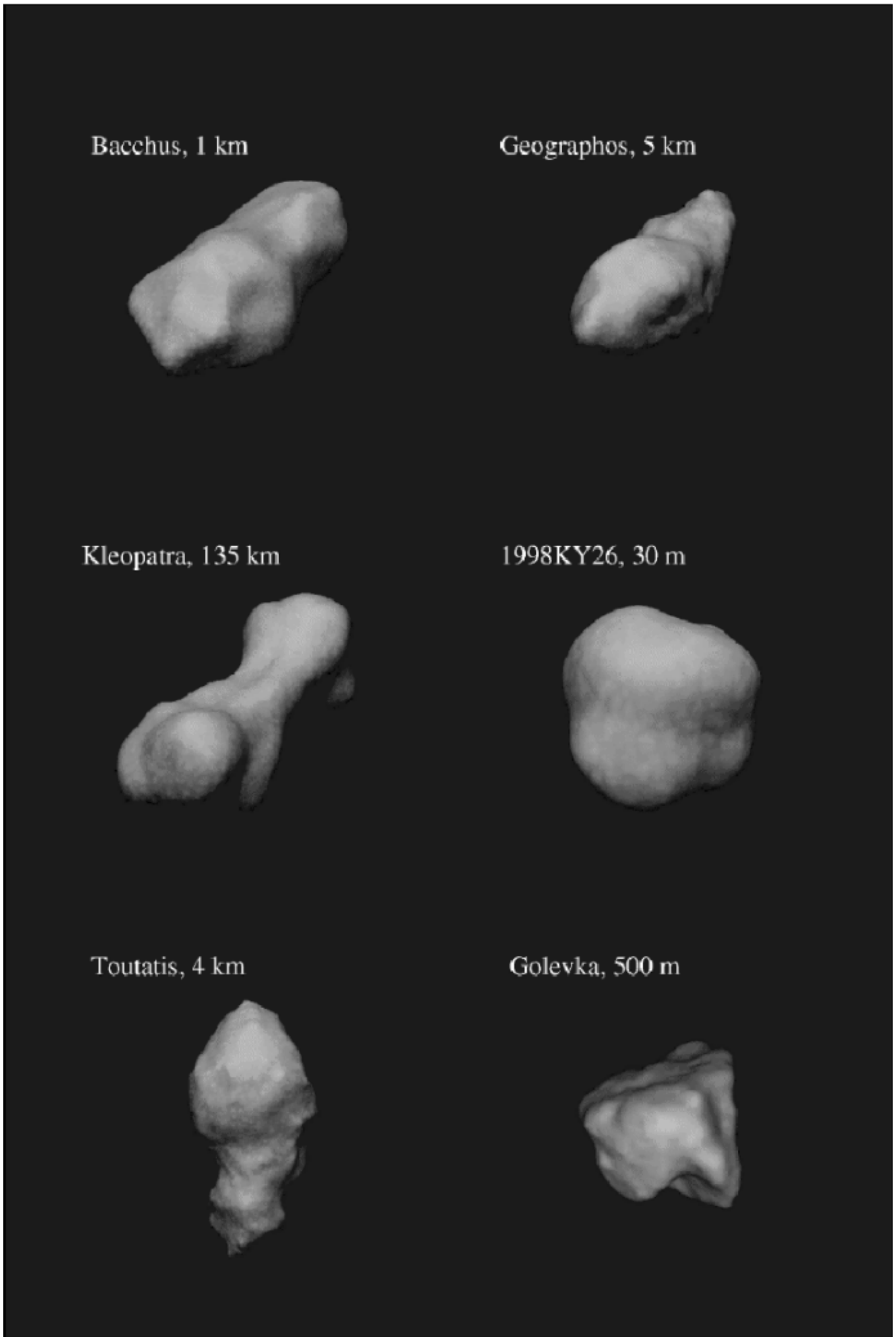

Figure 9. Shape models of five NEAs and one main-belt asteroid (Kleopatra), obtained by inverting Goldstone and Arecibo delay-Doppler images, or, in the case of 1998 KY26, CW spectra [*Hudson and Ostro*, *1995*; *Hudson et al.*, *2000a*; *Ostro et al.*, *2000b*].

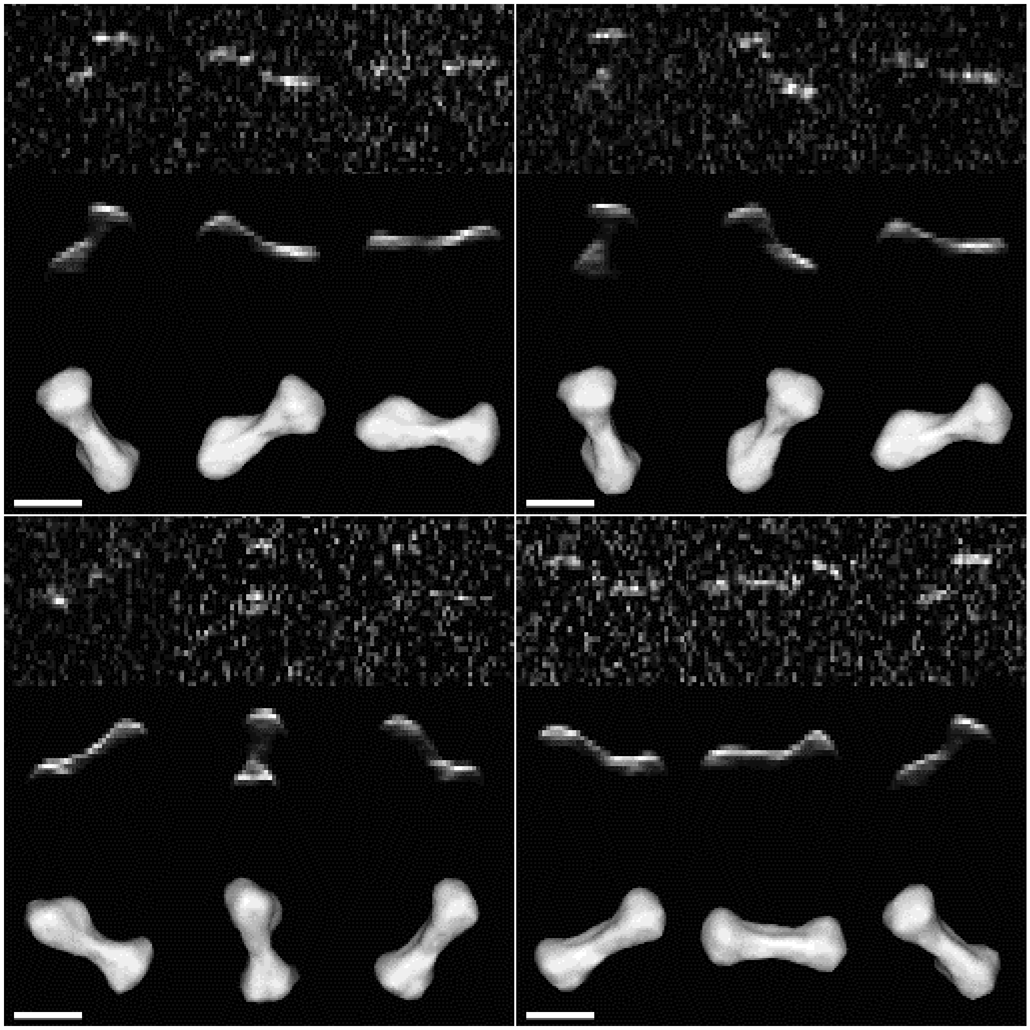

Figure 10. Shape-reconstruction results for the main-belt asteroid 216 Kleopatra. Each quadrant shows the Arecibo radar images from one day (top), the corresponding images calculated from the shape model, and the corresponding plane-of-sky views of the model (reprinted with permission from *S. J. Ostro et al.* [*2000b*], "Radar Observations of Asteroid 216 Kleopatra," *Science*, **288**, pp. 836-839; copyright 2000 American Association for the Advancement of Science).

ambiguities, the achievable resolutions with existing interferometer arrays that have adequate sensitivity is considerably worse that the resolution achievable with delay-Doppler imaging techniques. In 1991, *Slade et al.* [*1992*] used the Goldstone/VLA system to obtain full-disk images of Mercury, finding a very strong echo from the north polar region. The properties of the radar echo resembled those of echoes from the icy Galilean satellites [*Campbell et al.*, *1978*; *Ostro et al.*, *1992*], leading to the conclusion that there were probable ice deposits on the permanently-shadowed floors of impact craters near the poles of Mercury. As discussed above, *Harmon and Slade* [*1992*] had imaged Mercury during the same period, using the CLP technique, and were able to confirm the Goldstone/VLA result within a few days.

In 1991 and 1992, *de Pater et al.* [*1994*] used the Goldstone/VLA system to observe two main-belt asteroids, 324 Bamberga and 7 Iris, and two NEAs, 1991 EE and 4179 Toutatis, obtaining both spatial and spectral resolution to constrain the direction of their spin axes. While constraints on the spin-axis direction were obtained for both Bamberga and Iris, the VLA's spatial resolution of 0.24" in its most extended configuration, and the 381 Hz minimum channel resolution of its correlator, severely limits the applicability of this technique for asteroid observations. While the results obtained with the Goldstone/VLA radar-synthesis system have been both impressive and groundbreaking, it is unlikely that significantly improved observations of the terrestrial planets and smaller bodies will be possible until the current plans to extend the VLA and build a new correlator are realized.

An alternative to the VLA for synthesis imaging of NEAs and cometary nuclei is the Very Long Baseline Array (VLBA). The VLBA consists of ten 25 m antennas, distributed between Hawaii and the island of St Croix in the United States Virgin Islands. For an asteroid at 0.03 AU from the Earth, a not-unusual approach distance for a small NEA, the spatial resolution of the VLBA at 3.5 cm is ~ 25 m and, at 12.6 cm, it is ~ 100 m [*Black et al.*, *1999*]. While the promise of plane-of-sky resolutions of less than 100 m is exciting, there are significant problems that have to be overcome before the technique can be routinely used. The 10 VLBA antennas are equivalent to only an 80 m collecting area, so that, even for nearby objects, sensitivity is a problem, and the VLBA will need to be augmented by several larger antennas, such as the GBT, a phased VLA (3.5 cm only), Goldstone, and Arecibo. NEAs have typical rotation periods of only a few hours, so that integration times per image would need to be small. This results in a very "dirty" synthesized beam, given the small number of spatial Fourier components that could be measured, even with a few additional antennas. Current practical issues are the extreme near-field geometry for an object at a distance of only 0.03 AU (4.5×10^6 km), and the 124 Hz minimum channel resolution of the VLBA correlator. Even at 12.6 cm, the near-field distance of the VLBA is $\sim 5 \times 10^{11}$ km (3,000 AU). Some slowly rotating NEAs have Doppler-broadened bandwidths at 12.5 cm of about 1 Hz, so that the 124 Hz processing bandwidth reduces the signal-to-noise ratio by a factor of more than 10. While modifications to the correlator have been made to allow for observations of near-field objects, both this and the bandwidth problem would be most easily resolved if the correlations could be done in software, on standard computers. This will happen in the near future, once a device is completed that will copy data from the large-format instrumentation tapes of the standard VLBA recording system to a computer-compatible medium. Computer processing will allow high-resolution Doppler processing of the echo received by each antenna, reducing the synthesis imaging to a one-dimensional mapping, and reducing the problem of the "dirty" beam. Future enhancements could include transmitting a coded waveform and full delay-Doppler processing of the echo at each antenna. This would further reduce the mapping to just the set of points that contribute to the power in each delay-Doppler pixel in the image.

4. TOPOGRAPHY FROM INTERFEROMETRIC OBSERVATIONS

Over the past several years, there has been a revival of interest in using Earth-based radars for topographic measurements on the Moon and Venus, the two bodies where adequate signal-to-noise is available for such measurements. *Margot et al.* [*1999a*, *1999b*; *2000a*] utilized the Goldstone 3.5 cm wavelength radar to generate digital elevation models of Tycho crater and the polar regions of the Moon, with a spatial resolution of 150 m and a height resolution of about 50 m. Two efforts were made in 2001 to measure topography on Venus. *Slade et al.* [*2001*] used

Arecibo to transmit at 12.6 cm, and the Goldstone antennas as a receiving interferometer, to measure the topography near the sub-Earth point on the planet, while simultaneously solving for the N-S ambiguity problem. *Campbell et al.* [*private communication*] used Arecibo to transmit, and Arecibo and the 100 m GBT as a receiving interferometer, to measure the topography over the high-reflectivity regions of Maxwell Montes and Theia Mons, with higher spatial resolution than achieved by the Magellan altimeter. As of this writing, fringes have been detected for both the Arecibo/Goldstone and Arecibo/GBT observations, but no altitudes have yet been obtained for either measurement.

The use of Earth-based radar interferometers to measure altitudes on the Moon was first suggested and implemented by *Shapiro et al.* [*1972*]. Since that time, radar interferometry has been applied to terrestrial remote sensing [*Zebker and Goldstein*, *1986*], and has been used with considerable success for a variety of geophysical applications. Unlike terrestrial synthetic-aperture radar (SAR) applications, for almost all planetary radar observations, range-cell migration is not important, and unfocussed algorithms (i.e., simple delay-Doppler mapping) can be used. This is true for the Moon, if the spatial resolution and size of the image area are balanced.

Topography measurements, using a radar interferometer, are based on the rough orthogonality of the directions of changing delay, Doppler, and phase. The locus of points at the same distance from the radar on the surface of a solar-system body is defined by the intersection of a plane perpendicular to the line-of-sight vector with the surface of the body. The locus of points with the same Doppler shift is defined by the intersection with the surface of a plane parallel to the line-of-sight vector and the apparent rotation axis. For a receiving interferometer, where the projected baseline on the celestial sphere is roughly parallel to the apparent rotation axis, the direction of increasing fringe phase is approximately perpendicular to both the directions of changing range and Doppler shift, forming a roughly orthogonal system (Figure 11). Consequently, for any given point on the surface of the body, a measurement of its distance, Doppler shift, and relative fringe phase can be used to obtain its position in three dimensions. In the case of spherical bodies, such as the terrestrial planets and large satellites, these measurements can be compared with what would be expected for a smooth spherical or prolate surface, and the altitude can be determined. For an interferometer baseline of suitable extent and orientation, the spatial resolution and accuracy of the altitude measurement are determined almost entirely by signal-to-noise considerations.

As discussed above, points with given delay and Doppler values lie at the intersection of two orthogonal planes. These delay-Doppler lines are parallel to the apparent rotation axis, **k,** and are intersected by the fringe pattern of the interferometer as shown, in Figure 11. A measure of the interferometric phase, ϕ (i.e., the phase difference recorded by the two receivers forming the interferometer), can therefore be used to determine the elevation of each delay-Doppler resolution cell.

Figure 11 shows an arbitrary reflection element, located at $\mathbf{r} + \boldsymbol{\delta}\mathbf{r}$. In the mapping procedure [*Margot et al.*, *2000a*], one seeks estimates of the position, **r,** and elevation, $|\boldsymbol{\delta}\mathbf{r}|$, above a reference ellipsoid. These quantities can be measured from the observables – delay, τ, Doppler frequency, *f*, and interferometric phase, ϕ, – by the introduction of an imaginary point at a position $\mathbf{r}'$ with the same delay and Doppler values as the reflection element at position **r**. This point is chosen to be at zero elevation, and its imaginary interferometric phase, ϕ_0, can therefore be computed from ephemeris data.

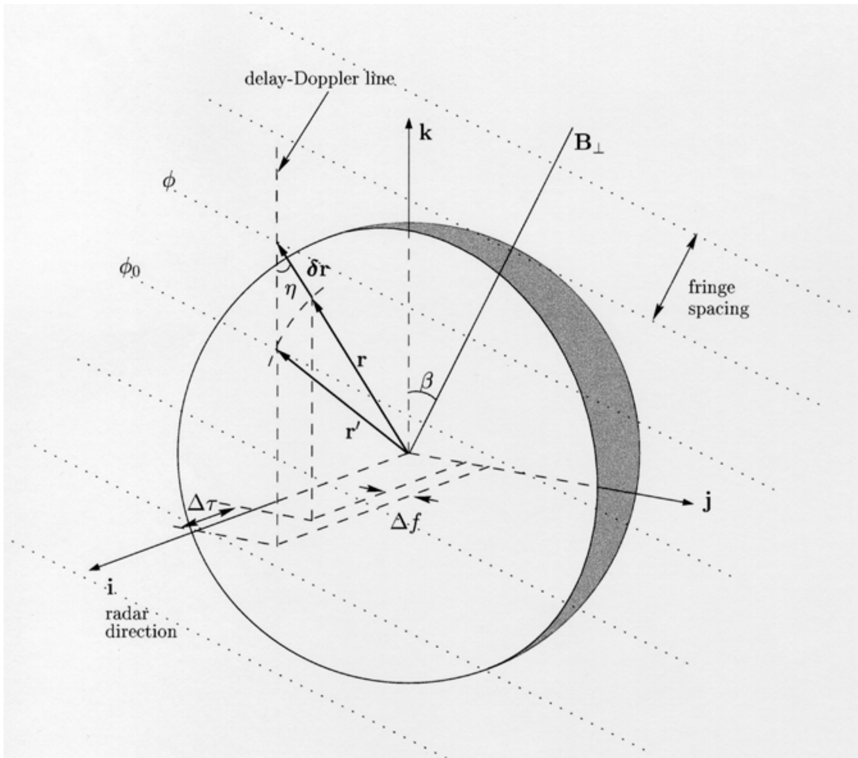

Figure 11. Interferometric phase measurements in the context of delay-Doppler imaging geometry. The fringe pattern of the interferometer (i.e., the loci of points with equal fringe phase) is shown by the dotted lines. The height of the reflection element, $|\boldsymbol{\delta}\mathbf{r}|$, induces changes $\Delta\tau$ and Δf in the delay and Doppler coordinates, compared with those of a point with the same latitude and longitude but zero elevation [*Margot et al., 2000a*].

The distance $|\mathbf{r}+\boldsymbol{\delta}\mathbf{r}-\mathbf{r}'|$ along the direction $\mathbf{k}$ can be derived from the difference between the measured phase, ϕ, at position $\mathbf{r}+\boldsymbol{\delta}\mathbf{r}$, and the computed phase, ϕ_0, at position $\mathbf{r}'$. This phase difference is shown to be equivalent to a fringe spacing, for ease of drawing, in Figure 11. The general relation is

$$|\mathbf{r}+\boldsymbol{\delta}\mathbf{r}-\mathbf{r}'| = \frac{\phi-\phi_0}{2\pi}\frac{s}{\cos\beta}, \tag{5}$$

where s is the fringe spacing, and β is the angle between the projected baseline, $\mathbf{B}_\perp$, and the apparent rotation axis, $\mathbf{k}$. Projection along the normal to the ellipsoid yields the height, $|\boldsymbol{\delta}\mathbf{r}|$:

$$|\mathbf{\delta r}| = |\mathbf{r} + \mathbf{\delta r} - \mathbf{r}'|\cos\eta \,. \tag{6}$$

In this last transformation, the required angular separation between the normal, **r**, and direction **k** is not known a priori. A very good estimate of the angle η is given by the separation between $\mathbf{r}'$ and **k**. This approximation is legitimate, since topographic changes represent a very small fraction of the planetary radius, and $\mathbf{r}'$ is expected to be nearly aligned with **r**. The approximation breaks down at low incidence angles, in a region where radar imaging is avoided if at all possible, because of ambiguity difficulties.

The height, $|\mathbf{\delta r}|$, above the sphere is assigned to the delay-Doppler coordinate of the element under consideration. Note that these delay and Doppler values are different from those of a zero-elevation point, located at the same latitude and longitude, as illustrated in Figure 11. A coordinate transformation between delay-Doppler space and latitude-longitude space would therefore result in geometric distortions (e.g., foreshortening), if it did not take topography into account.

The process of registering a radar map to a specific cartographic projection, with due account being taken for the elevation-induced distortions, requires correction to the delay and Doppler values, which can be computed from a knowledge of $\mathbf{\delta r}$. The corrections are

$$\Delta\tau = \frac{2}{c}\left(\mathbf{\delta r}\bullet\mathbf{i}\right), \tag{7}$$

$$\Delta f = \frac{2}{\lambda}\omega\left(\mathbf{\delta r}\bullet\mathbf{j}\right), \tag{8}$$

where **i** and **j** are the vectors indicated in Figure 11. These corrections can be implemented to produce digital elevation models and radar images, properly rectified and free of elevation-induced distortions.

For measurements of the topography of the Moon, utilizing either the Arecibo or Goldstone radar systems, delay-Doppler ambiguity issues are not relevant, except very close to the mean sub-Earth latitude and longitude. This is because the transmitting-antenna beams only subtend about 350 km on the surface of the Moon, much smaller than the spacing between almost all pairs of ambiguity points. Signal-to-noise considerations allow measurements at high spatial and height resolutions, out to incidence angles of 90°. For Venus, with the possible exception of small areas of very high backscatter cross section at high elevations, signal-to-noise considerations dictate that topographic measurements must be made near the sub-Earth point (incidence angle close to zero), where the backscatter cross section is very high, due to the presence of a specular component in the scattering law. This means that a receiving interferometer must be used simultaneously to solve for the N-S ambiguity and to obtain the topography. A pair of antennas cannot achieve both of these from a single "instantaneous" (i.e., one-look) observation. *Rumsey et al.* [*1974*] pointed out that it can be done with a multiple-baseline interferometer system, obtained either by using several suitably spaced receiving antennas, or by combining multiple observations with different projected baselines, using a pair of antennas.

Margot et al. [*1999a*] demonstrated the potential of the current Earth-based radar systems for topographic measurements of the Moon by producing a digital elevation model (DEM) of the

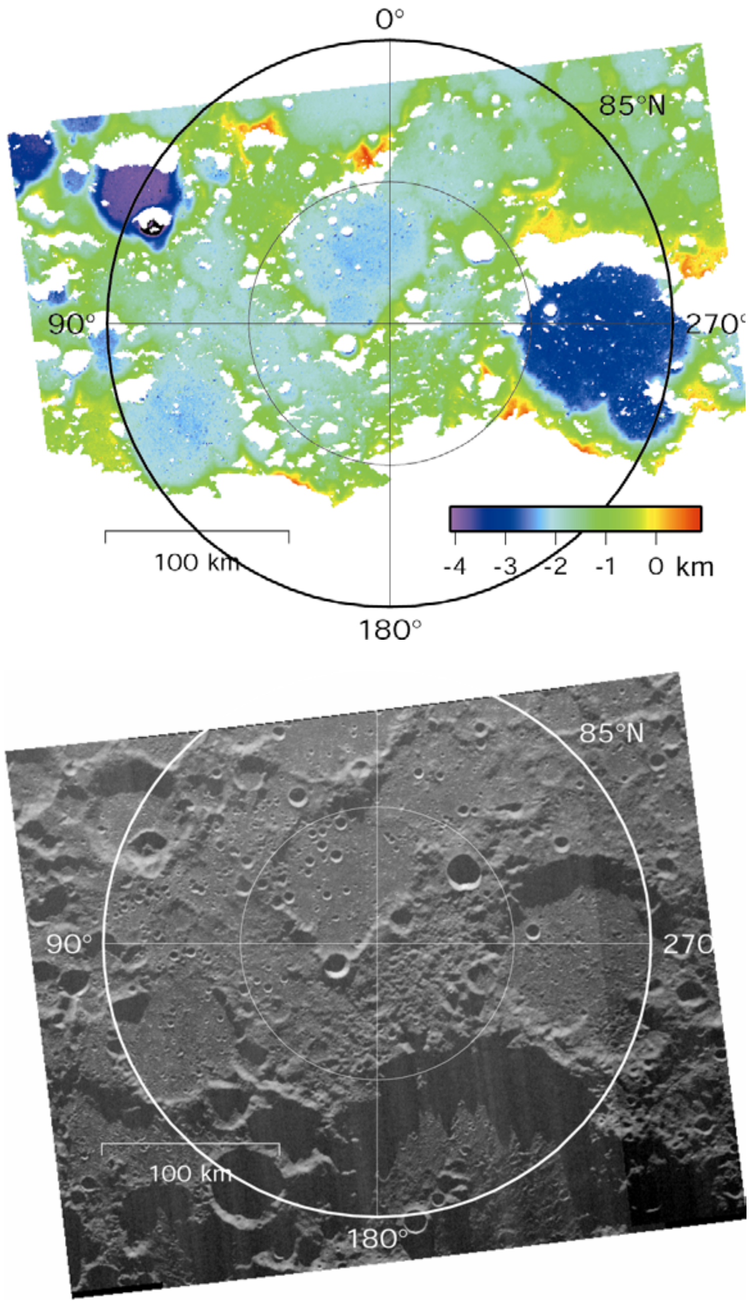

Figure 12. A digital-elevation model (top) and radar-backscatter map (bottom) of the north-polar region of the Moon, derived from Goldstone radar-interferometric observations. The elevations are with respect to a sphere with a radius of 1738 km. The spatial resolution is 150 m, and the height resolution is approximately 50 m (reprinted with permission from *J. L. Margot et al.* [*1999b*], "The Topography of the Lunar Poles from Radar Interferometry: A Survey of Cold Trap Locations," *Science*, **284**, pp. 1658-1660, copyright 1999, American Association for the Advancement of Science) (also see Plate 16 for top image).

Tycho crater, using the 3.5 cm radar transmitter on the 70 m NASA/DSN Goldstone antenna, and three nearby 34 m antennas making up the receiving interferometer. Reference heights were obtained using the laser-altimeter tracks of the Clementine orbiter, which are spaced approximately 2.7° apart in longitude. The spatial and height resolutions were 150 m and 50 m, respectively. *Margot et al.* [*1999b*] then proceeded to apply the technique to the polar regions of the Moon (Figure 12). There were no topographic measurements for the poles, and, due to the suggestion that water ice may exist in areas of permanent shadow, considerable interest in the location of these areas. These areas were delineated by ray tracing, using the polar DEMs [*Margot et al.*, *1999b*].

5. POLARIZATION AND WAVELENGTH DEPENDENCE

The polarization properties of the radar signal reflected from a surface are determined by the nature of the scattering process, and, hence, contain information about the physical and electrical properties of the target-body's surface. Early work on the Moon by *Hagfors et al.* [*1965*] and, more recently, by *Stacy* [*1993*] derived dielectric constants and other properties of the lunar regolith from measurements of the full Stokes'-parameters polarization properties of the reflected echo. *Carter et al.* [*2001*] have used the upgraded Arecibo radar to do similar measurements on Venus. These were aimed at measuring dielectric constants for terrain types such as extended crater-ejecta deposits, and wind-blown deposits where there is significant penetration of the incident wave into the surface. However, sensitivity considerations have largely limited the use of polarization information to what can be obtained from measurements of the circular-polarization ratio. Almost all planetary radar observations are done by transmitting a circularly polarized signal, and receiving the echo in both the sense of circular polarization expected for a mirror-like reflection, the sense opposite (OC) from that transmitted, and in the same (SC) sense as that transmitted. Echo power in the SC sense arises from multiple scattering, scattering from wavelength-scale surface or subsurface structures, and – for penetration into low-porosity surfaces such as the lunar regolith – from the differences in the linear-polarization transmission coefficients perpendicular and parallel to the plane of incidence. The circular polarization ratio, μ_c, is defined as the ratio of the received power in the SC sense of circular polarization to that in the OC sense. For a perfectly specular surface, normal to the line-of-sight, all of the received power would be in the OC sense, giving a μ_c of zero. In contrast, for a perfectly diffuse surface, the echo power would be equally divided between the OC and SC senses of received polarization, giving a μ_c of unity. Therefore, a measurement of μ_c is indicative of the degree of diffuse scattering, and is typically used to provide an estimate of the relative roughness of the scattering surface at wavelength scales. For surfaces such as those of the terrestrial planets and many asteroids, with values for μ_c of less than approximately 0.1, most of the echo power is in the specular component. This allows the backscatter cross section to be used to estimate the Fresnel reflectivity of the body's surface material. The reflectivity can then be used to obtain the dielectric constant. This can be used to either constrain the composition or, for powdered surfaces, to estimate the degree of porosity of the surface material [see, e.g., *Ostro et al.*, *2000b*].

Studies of the wavelength dependence of scattering from solar-system bodies are another area that has received little attention in recent years. This is at least partly due to the limited number of current active systems, and, hence, the limited number of wavelengths in use. For near-nadir measurements of the quasi-specular echo from surfaces, the Hagfors' scattering law [*Hagfors*, *1964*] is normally fitted to the data to derive rms slopes. However, this scattering function is wavelength independent, and the values of the derived rms slopes can be dependent on the wavelength used. Recently, *Shepard and Campbell* [*1999*] have derived a wavelength-dependent scattering model, based on a self-affine fractal description of the scattering surface.

For Europa, Ganymede, and Callisto, the icy Galilean satellites of Jupiter, multi-wavelength, 3.5 cm, 12.6 cm, and 70 cm measurements of their radar-scattering properties have been used to investigate the sub-surface structures responsible for their unusual radar-scattering properties. The discovery, in the 1970s, that these icy satellites have normalized-backscatter cross sections that are greater than unity (i.e., they preferentially scatter the radar signal back towards the radar), and values for μ_c greater than unity [*Campbell et al.*, *1977*, *1978*], was a considerable surprise. No other terrestrial surface or solar-system body had exhibited such behavior. A number of suggestions were made to explain these values, based either on reflections from surface structures or subsurface scatter, or refraction effects combined with long path lengths, due to the very low attenuation of radio waves in ice at this temperature. None of these suggestions was entirely convincing, until *Hapke* [*1990*] pointed out that the radar properties could be due to a coherent-backscatter effect that had been discovered at optical wavelengths. In this process, the high backscatter cross section is related to subsurface scatter and the coherent addition of the emergent signal, corresponding to one ray path and its time reversed equivalent. This addition only occurs in the backscatter direction, and only for very small angles about it, dependent on the signal path-length in the ice. A summary of the Arecibo 13 cm and Goldstone 3.5 cm observational results on the icy Galilean satellites was published by *Ostro et al.* [*1992*].

Recent observational work on the icy Galilean satellites has involved measurements of their backscattering properties at 70 cm wavelength [*Black et al.*, *2001a*], using the Arecibo 70 cm radar system. These data, plus the equivalent measurements at 3.5 and 12.6 cm, were used by *Black et al.* [*2001b*] as inputs to a coherent-backscatter model. This model was developed by *Peters* [*1992*], and modified to include predictions of the backscatter cross section to obtain estimates of the number-size distributions of the subsurface scatterers, responsible in Peters' model for the radar echo, and the depths of the scattering layers for the three satellites.

6. FUTURE PROSPECTS

6.1 Short Term

Over the next decade, there is little prospect for substantial improvements in the sensitivity of any of the current planetary radar systems, and even less prospect for building a new, more-powerful system. Small improvements in gain and system temperature for the Arecibo 2380 MHz system could provide up to 2 db increase in sensitivity, relative to the system as of December, 2001 (the parameters in Table 1). Both gain and system temperature for the Goldstone 8560 MHz system are already optimized, and virtually no improvement is anticipated. However, there are (currently unfunded) plans to double the power of the transmitter of the Goldstone system to about 1.0 MW, giving a 3 db increase in sensitivity. This will require the use of four klystrons, and the complexity of combining their outputs.

For a given antenna, one method of increasing the sensitivity of the radar system is to change to a shorter wavelength. The wavelength dependence of sensitivity for a monostatic system, for essentially all planetary radar observations, is given by

$$Sensitivity \propto P\lambda^{-3/2}\eta^2 \big/ T_{sys}, \tag{9}$$

where P is the transmitter power, λ is the wavelength, η is the antenna-aperture efficiency, and T_{sys} is the system temperature. For Arecibo, assuming a rms accuracy for the primary reflector of 2.0 mm, the expected improvement in sensitivity in changing from the current wavelength of 12.6 cm to 6.0 cm would be approximately 2.3. Going to 3.5 cm, the change would be a factor of approximately 2.7. That these increases are not larger is due to the reduction in aperture efficiency at the shorter wavelengths. However, assuming no change in transmitter power and system temperature, a further factor of two increase in sensitivity is feasible. This may be difficult, or, at least, expensive to achieve, as 500 kW output-power klystrons are not available at these wavelengths. In theory, the wavelength of the Goldstone system could be reduced from its current 3.5 cm but, in practice, it would not be possible at present to maintain the current 500 kW power level at a significantly shorter wavelength, without a considerable development effort.

There are plans to change the wavelength of the Evpatoria radar from its current 6 cm to 3.5 cm, and to increase the transmitter power to 1.0 MW. Assuming state-of-the-art receivers, or reception with the 100 m Effelsberg telescope, this system would be competitive with the Goldstone radar system, and capable of making significant contributions to the field of radar astronomy.

In the absence of significant sensitivity increases in the short term, advances in the field will depend on innovative use of current systems, including alternative receiving antennas, and further development of data-analysis and inversion techniques. The application of interferometry and synthesis-imaging techniques to the investigation of asteroids and cometary nuclei has promise for providing plane-of-sky images of these objects. For the long-baseline synthesis imaging to be truly successful, a number of large antennas – the GBT, Arecibo, and the VLA, for example – need to be used in conjunction with the VLBA to increase sensitivity. As discussed in Section 3, to achieve resolutions of 20 m or better in two dimensions, it will be necessary to use coded transmissions, and to carry out a full delay-Doppler analysis for the data from each antenna. The synthesis analysis would then be used to determine the plane-of-sky locations and backscatter cross sections of each range-Doppler element.

6.2 Longer Term

In 10 to 15 years, two projects that are in the planning stage could provide significant improvements in sensitivity and/or resolution. The planned expansion of the VLA (the EVLA) would add eight or 10 new antennas, providing baselines up to 300 km, and would also connect to the existing VLBA, for a total of up to 47 antennas. The EVLA, with its 35 or 37 antennas, will allow imaging of the terrestrial planets with six times the resolution of the existing VLA synthesis images, and measurements of the rotation states of main-belt asteroids. The combined arrays would significantly improve the synthesis imaging of NEAs, as discussed in Section 3. The international project to build a cm-wavelength synthesis array with a very large collecting area –

the Square Kilometer Array, or SKA – provides an opportunity for a planetary radar system with significantly greater sensitivity than current systems. Current thinking is that there would be a separate transmitting facility, possibly an array, with small transmitters providing power for each element. If the transmitting module has an area equivalent to a 100 m-diameter dish, with an aperture efficiency at, say, 10 GHz of 70%, and the transmitter power was 1.0 MW, then the combination of this transmitting facility with the square-kilometer receiving area of the array would result in a radar system with approximately 20 times (13 db) the sensitivity of the current Arecibo system. What could be achieved with such a system?

Asteroids and comets: The SKA would have a substantial imaging capability for NEOs, and, to a lesser extent, main-belt asteroids. For a 1.0 km-diameter asteroid – at a distance of 0.1 AU from the Earth, and with typical values of its radar albedo and rotation period of 0.1 and 5 hr, respectively – the signal-to-noise ratio with this radar system after 100 seconds of integration would be approximately 10^4. This would allow imaging with 10 to 20 m resolution. For comets, the typical radar albedo is closer to 0.04, reducing the expected signal-to-noise ratio to about 4×10^3. The 100 sec integration period corresponds to a rotation by about one resolution cell, assuming the 5 hr period. A baseline of 1000 km is approximately 3×10^7 wavelengths long at 10 GHz. This corresponds to a spatial resolution at 0.1 AU of 500 m. Even at 20 GHz, the highest currently discussed frequency of the SKA, the resolution would still be only 250 m. Consequently, to achieve the 10 to 20 m resolution allowed by signal-to-noise considerations, coded waveforms will be needed, with the synthesis-imaging capability of the array being used to resolve range-Doppler ambiguities.

For asteroids in the main belt, the achievable resolutions from both signal-to-noise and synthesized-beam resolution considerations are more evenly matched, and the SKA would be the premier instrument for studying these bodies.

Terrestrial planets: At the distances of the closest approaches of Mercury, Venus, and Mars to the Earth, the best spatial resolution of the SKA will be approximately 4 km, 1.5 km, and 2 km, respectively. The SKA-based radar system would be capable of imaging the surface of Mercury at 4 km resolution, with a 1.0-sigma sensitivity limit of about –30 db. For Mars, the equivalent spatial resolution for the same sensitivity limit would be 2 km. Unfortunately, the very high absorption in the Venus atmosphere at 10 GHz would prevent good imaging of the surface. For both Mercury and Mars, radar images at 2 to 4 km resolution would potentially be of great interest.

Satellites of the outer planets: At the distance of the Jupiter system – at its closest approach to the Earth, at a distance of about 4.2 AU – the lowest spatial size of the SKA's synthesized beam would be about 25 km. Given the very high backscatter cross sections of the icy Galilean satellites, signal-to-noise considerations would allow imaging with about 100 km resolution. Consequently, the SKA would allow unambiguous imaging of the icy satellites with this resolution. With the possible exception of Europa, there are no current plans for a radar-equipped spacecraft to investigate the unusual radar-scattering properties of these satellites, so SKA observations would be a major objective. An SKA system could also be used to investigate the radar-scattering properties of some of the smaller satellites of Jupiter and Saturn.

7. ACKNOWLEDGEMENTS

The authors gratefully acknowledge P. Nicholson, for helpful comments on the manuscript, and G. Black and J. Harmon, for assistance with the figures. D. Campbell and R. S. Hudson are partially supported under grants from NASA. The National Astronomy and Ionosphere Center is operated by Cornell University, under a cooperative agreement with the US National Science Foundation, and with support from NASA.

8. REFERENCES

A. K. Andrews, R. S. Hudson, and D. Psaltis [1995], "Optical-Radar Imaging of Scale Models for Studies in Asteroid Astronomy," *Optics Letters*, **20**, pp. 2327-2329.

L. A. M. Benner, S. J. Ostro, J. D. Giorgini R. F. Jurgens, J. L. Margot, and M. C. Nolan [2001a], "1999 KW4," *IAU Circ*. No. 7632.

L. A. M. Benner, M. C. Nolan, S. J. Ostro, J. D. Giorgini, and J. L. Margot [2001b], "1999 ST27," *IAU Circ*. No. 7730.

L. A. M. Benner, S. J. Ostro, M. C. Nolan, J. L. Margot, J. D. Giorgini, R. S. Hudson, R. F. Jurgens, M. A. Slade, E. S. Howell, D. B. Campbell, and D. K. Yeomans [2001c], "Radar Observations of Asteroid 1999 JM8," *Meteorites and Planetary Science*, in press (publication expected June, 2002).

G. J. Black, D. B. Campbell, B. Butler, and S. J. Ostro [1999], "Plans for VLBA-Radar Imaging of Near-Earth Objects," (abstract), Asteroids, Meteors and Comets Conference (available from the Department of Astronomy, Cornell University, Ithaca, New York 14853-6801).

G. J. Black, D. B. Campbell, and S. J. Ostro [2001a], "Icy Galilean Satellites: 70 cm Radar Results from Arecibo," *Icarus*, **151**, pp. 160-166.

G. J. Black, D. B. Campbell, and P. D. Nicholson [2001b], "Icy Galilean Satellites: Modeling Radar Reflectivities as a Coherent Backscatter Effect," *Icarus*, **151**, pp. 167-180.

D. B. Campbell, J. F. Chandler, G. H. Pettengill, and I. I. Shapiro [1977], "Galilean Satellites of Jupiter: 12.6-Centimeter Radar Observations," *Science*, **196**, pp. 650-653.

D. B. Campbell, J. F. Chandler, S. J. Ostro, G. H. Pettengill, and I. I. Shapiro [1978], "Galilean Satellites: 1976 Radar Results," *Icarus*, **34**, pp. 254-267.

L. M. Carter, D. B. Campbell, J. L. Margot, B. A. Campbell, and J. Dorris [2001], "Surface Properties of Venus from Arecibo 12.6 cm Radar Observations," (abstract), Lunar and Planetary Science Conference XXXII (available from the Lunar and Planetary Institute, 3600 Bay Area Boulevard, Houston, TX 77058-1113).

I. de Pater, P. Palmer, D. L. Mitchell, S. J. Ostro, and D. K. Yeomans [1994], "Radar Aperture Synthesis Observations of Asteroids," *Icarus*, **111**, pp. 489-502.

T. Hagfors [1964], "Backscattering from an Undulating Surface with Applications to Radar Returns from the Moon," *J. Geophys. Res.*, **69**, pp. 3779-3784.

T. Hagfors, R. A. Brockelman, H. H. Danforth, L. B. Hanson, and G. M. Hyde [1965], "Tenuous Surface Layer on the Moon: Evidence Derived from Radar Observations," *Science*, **150**, pp. 1153-1156.

T. Hagfors and W. Kofman [1991], "Mapping of Overspread Targets in Radar Astronomy," *Radio Science*, **26**, pp. 403-416; (corrigenda: T. Hagfors and W. Kofman [1992], *Radio Science*, **27**, p. 232.)

B. W. Hapke [1990], "Coherent Backscatter and the Radar Characteristics of Outer Planet Satellites," *Icarus*, **88**, pp. 407-417.

L. J. Harcke, H. A. Zebker, R. F. Jurgens, M. A. Slade, B. J. Butler, and J. K. Harmon [2001], "Radar Observations of the Icy Galilean Satellites During the 2000 Opposition," (abstract), Lunar and Planetary Science Conference XXXII (available from the Lunar and Planetary Institute, 3600 Bay Area Boulevard, Houston, TX 77058-1113).

J. K. Harmon and M. A. Slade [1992], "Radar Mapping of Mercury: Full-Disk Images and Polar Anomalies," *Science*, **258**, pp. 640-643.

J. K. Harmon, M. P. Sulzer, P. J. Perillat, and J. F. Chandler [1992], "Mars Radar Mapping: Strong Backscatter from the Elysium Basin and Outflow Channel," *Icarus*, **95**, pp. 153-156.

J. K. Harmon, S. J. Ostro, J. F. Chandler, and R. S. Hudson [1994], "Radar Ranging to Ganymede and Callisto," *Astronomical Journal*, **107**, pp. 1175-1181.

J. K. Harmon [1997], "Mercury Radar Studies and Lunar Comparisons," *Advanced Space Research*, **19**, 10, pp. 1487-1496.

J. K. Harmon, R. E. Arvidson, E.A. Guinness, B. A. Campbell, and M. A. Slade [1999], "Mars Mapping with Delay-Doppler Radar," *Journal of Geophysical Research*, **104**, pp. 14065-14090.

J. K. Harmon, P. J. Perillat, and M. A. Slade [2001], "High-Resolution Radar Imaging of Mercury's North Pole," *Icarus*, **149**, pp. 1-15.

J. K. Harmon [2001], "Planetary Delay-Doppler Radar and the Long Code Method," *IEEE Transactions on Geoscience and Remote Sensing*, submitted for publication.

R. S. Hudson [1993], "Three-Dimensional Reconstruction of Asteroids from Radar Observations," *Remote Sensing Reviews*, **8**, pp. 195-203.

R. S. Hudson and S. J. Ostro [1994], "Shape of Asteroid 4769 Castalia (1989 PB) from Inversion of Radar Images," *Science*, **463**, pp. 940-943.

R. S. Hudson and S. J. Ostro [1995], "Shape and Non-Principal Axis Spin State of Asteroid 4179 Toutatis," *Science*, **270**, pp. 84-86.

R. S. Hudson, S. J. Ostro, et al. [2000a], "Radar Observations and Physical Model of 6489 Golevka," *Icarus*, **48**, pp. 37-51.

R. S. Hudson, S. J. Ostro, and L. A. Benner [2000b], "Recent Delay-Doppler Radar Asteroid Modeling Results: 1999 RQ36 and Craters on Toutatis," (abstract), Division of Planetary Sciences Meeting, paper 32.0710H (available from the American Astronomical Society)

R. F. Jurgens, A. F. C. Haldemann, and M. A. Slade [2001], "GSSR Mars Delay-Doppler Data Available for MER Landing Site Assessment," Lunar and Planetary Science Conference XXXII (available from the Lunar and Planetary Institute, 3600 Bay Area Boulevard, Houston, TX 77058-1113).

P. S. Kildal, L. A. Baker, and T. Hagfors [1994], "The Arecibo Upgrading: Electrical Design and Expected Performance of the Dual-Reflector Feed System," *Proceedings of the IEEE*, **82**(5), pp. 714-724.

J. L. Margot and M. Nolan [1999], "Radar Interferometric Imaging of 6489 Golevka," (abstract), Asteroids, Meteors and Comets Conference (available from the Department of Astronomy, Cornell University, Ithaca, New York 14853-6801).

J. L. Margot, D. B. Campbell, R. F. Jurgens, and M. A. Slade [1999a], "The Topography of Tycho Crater," *Journal of Geophysical Research*, **104**, pp. 11875-11882.

J. L. Margot, D. B. Campbell, R. F. Jurgens, and M. A. Slade [1999b], "The Topography of the Lunar Poles from Radar Interferometry: A Survey of Cold Trap Locations," *Science*, **284**, pp. 1658-1660.

J. L. Margot, D. B. Campbell, R. F. Jurgens, and M. A. Slade [2000a], "Digital Elevation Models of the Moon from Earth-based Radar Interferometry," *IEEE Transactions on Geoscience and Remote Sensing*, **38**, 2, pp. 1122-1133.

J. L. Margot, M. C. Nolan, L. A. M. Benner, S. J. Ostro, R. F. Jurgens, M. A. Slade, J. D. Giorgini, and D. B. Campbell [2000b], "2000 DP107," *IAU Circ*. No. 7503.

J. L. Margot, M. C. Nolan, L. A. M. Benner, S. J. Ostro, R. F. Jurgens, J. D. Giorgini, M. A. Slade, and D. B. Campbell [2002], "Binary Asteroids in the Near-Earth Object Population," *Science*, **296**, pp. 1445-1448.

D. O. Muhleman, B. J. Butler, A. W. Grossman, and M. A. Slade [1991], "Radar Images of Mars," *Science*, **253**, pp. 1508-1513.

P. D. Nicholson, D. B. Campbell, R. G. French, G. J. Black, J. L. Margot, and M. Nolan [2000], "Radar Images of Saturn's Rings," *Bulletin of the American Astronomical Society*, **32**, p. 1086.

M. C. Nolan, J. L. Margot, E. S. Howell, L. A. M. Benner, S. J. Ostro, R. F. Jurgens, J. D. Giorgini, and D. B. Campbell [2000], "2000 UG11," *IAU Circ*. No. 7518.

S. J. Ostro, G.H. Pettengill, D. B. Campbell, and R. M. Goldstein [1982], "Delay-Doppler Radar Observations of Saturn's Rings," *Icarus*, **49**, pp. 367-381.

S. J. Ostro, D. B. Campbell, R. A. Simpson, R. S. Hudson, J. F. Chandler, K. D. Rosema, I. I. Shapiro, E. M. Standish, R. Winkler, D. K. Yeomans, R. Velez, and R. M. Goldstein [1992], "Europa, Ganymede, and Callisto: New Radar Results from Arecibo and Goldstone," *Journal of Geophysical Research*, **97**, E11, pp. 18227-18244.

S. J. Ostro, J. L. Margot, M. C. Nolan, L. A. M. Benner, R. F. Jurgens, and J. D. Giorgini [2000a], "2000 DP107," *IAU Circ*., No. 7496.

S. J. Ostro, R. S. Hudson, M. C. Nolan, J. L. Margot, D. J. Scheeres, D. B. Campbell, C. Magri, J. D. Giorgini, and D. K. Yeomans [2000b], "Radar Observations of Asteroid 216 Kleopatra," *Science*, **288**, pp. 836-839.

K. Peters [1992], "The Coherent Backscatter Effect: A Vector Formulation Accounting for Polarization and Absorption Effects and Small or Large Scatterers," *Phys. Rev. B*, **46**, pp. 801-812.

I. I. Shapiro, S. H. Zisk, A. E. E. Rogers, M. A. Slade, and T. W. Thompson [1972], "Lunar Topography: Global Determination by Radar," *Science*, **178**, pp. 939-948.

M. K. Shepard and B. A. Campbell [1999], "Radar Scattering from a Self-Affine Fractal Surface: Near-Nadir Regime", *Icarus*, **141**, pp. 156-171.

M. A. Slade, B. J. Butler, and D. O. Muhleman [1992], "Mercury Radar Imaging: Evidence for Polar Ice," *Science*, **258**, pp. 635-640.

M. A. Slade, M. Simons, M. E. Pritchard, and R. F. Jurgens [2001], "Arecibo to Goldstone Radar Interferometric Topography of Selected Regions of Venus," (abstract no. 1511), Lunar and Planetary Science Conference XXXII (available from the Lunar and Planetary Institute, 3600 Bay Area Boulevard, Houston, TX 77058-1113).

N. J. S. Stacy [1993], "High-Resolution Synthetic Aperture Radar Observations of the Moon," Cornell University PhD Thesis.

N. J. S. Stacy, D. B. Campbell, and P. G. Ford [1997], "Arecibo Radar Mapping of the Lunar Poles: A Search for Ice Deposits," *Science*, **276**, pp. 1527-1530.

M. P. Sulzer [1986], "A Radar Technique for High Range Resolution Incoherent Scatter Autocorrelation Function Measurements Utilizing the Full Average Power of Klystron Radars," *Radio Science*, **21**, pp. 1033-1040.

H. A. Zebker and R. M. Goldstein [1986], "Topographic Mapping from Interferometric Synthetic Aperture Radar Observations," *Journal of Geophysical Research*, **91**, pp. 4993-4999.